CANCER IMMUNOLOGY

Combination cancer immunotherapy targeting PD-1 and GITR can rescue CD8$^+$ T cell dysfunction and maintain memory phenotype

Bei Wang*, Wen Zhang*, Vladimir Jankovic, Jacquelynn Golubov, Patrick Poon, Erin M. Oswald, Cagan Gurer, Joyce Wei, Ilyssa Ramos, Qi Wu, Janelle Waite, Min Ni, Christina Adler, Yi Wei, Lynn Macdonald, Tracey Rowlands, Susannah Brydges, Jean Siao, William Poueymirou, Douglas MacDonald, George D. Yancopoulos, Matthew A. Sleeman, Andrew J. Murphy, Dimitris Skokos†

Most patients with cancer do not develop durable antitumor responses after programmed cell death protein 1 (PD-1) or programmed cell death ligand 1(PD-L1) checkpoint inhibition monotherapy because of an ephemeral reversal of T cell dysfunction and failure to promote long-lasting immunological T cell memory. Activating costimulatory pathways to induce stronger T cell activation may improve the efficacy of checkpoint inhibition and lead to durable antitumor responses. We performed single-cell RNA sequencing of more than 2000 tumor-infiltrating CD8$^+$ T cells in mice receiving both PD-1 and GITR (glucocorticoid-induced tumor necrosis factor receptor–related protein) antibodies and found that this combination synergistically enhanced the effector function of expanded CD8$^+$ T cells by restoring the balance of key homeostatic regulators CD226 and T cell immunoreceptor with Ig and ITIM domains (TIGIT), leading to a robust survival benefit. Combination therapy decreased CD8$^+$ T cell dysfunction and induced a highly proliferative precursor effector memory T cell phenotype in a CD226-dependent manner. PD-1 inhibition rescued CD226 activity by preventing PD-1–Src homology region 2 (SHP2) dephosphophorylation of the CD226 intracellular domain, whereas GITR agonism decreased TIGIT expression. Unmasking the molecular pathways driving durable antitumor responses will be essential to the development of rational approaches to optimizing cancer immunotherapy.

INTRODUCTION

After the initial clinical successes obtained using programmed cell death protein 1 (PD-1) and cytotoxic T lymphocyte–associated antigen 4 (CTLA-4) antibody (Ab) treatments in patients with cancer, the number of immunotherapy agents in clinical development is expanding rapidly with goals of improving the limited response rate and generating more durable responses (*1*, *2*). Recent elegant studies using infectious disease–related mouse models demonstrated that PD-1 blockade induces an incomplete rescue of exhausted T cells (T_{Exs}), thus failing to restore T_{Exs} into T effector memory cells (T_{EMs}), which are required for an effective immune memory (*3*, *4*). Although PD-1 and/or programmed cell death ligand 1 (PD-L1) inhibition affects the transcriptional and epigenetic landscape of T_{Exs}, these cells are not fully reprogrammed when antigen concentration remains high and fail to acquire a memory phenotype upon antigen clearance (*3*). Designing additional strategies to induce more robust T cell activation and/or target other immunoregulatory pathways could contribute to the generation of sustainable long-term responses.

Combination treatments aimed at PD-1 inhibition and activation of costimulatory receptor GITR [glucocorticoid-induced tumor necrosis factor receptor (TNFR)–related protein or TNFRSF18] to induce a stronger T cell activation are currently being evaluated in early-phase clinical trials for patients with metastatic melanoma and other solid tumors (*5*, *6*). Although the intrinsic properties of each Ab and the selection of the appropriate indications for use play an important role in the clinical outcome, emerging data from a small clinical study reported limited clinical activity for anti-GITR monotherapy and potentially promising data for the combination therapy (*7*). In preclinical studies in which monotherapy with anti-GITR or anti–PD-1 Ab has limited efficacy (e.g., in large or poorly immunogenic murine tumors) (*6*, *8*), combination therapy was able to achieve long-term survival in mouse models of ovarian and breast cancer (*9*). However, the effect of this synergism on T cell dysfunction and the underlying molecular mechanisms remain unknown. Here, we sought to establish an experimental approach to identify the mechanisms of antitumor synergism between anti-GITR and anti–PD-1 Abs. We genetically profiled more than 2000 tumor-infiltrating CD8$^+$ T cells in the murine MC38 colon adenocarcinoma model using single-cell T cell receptor (TCR) and transcriptome sequencing. Our systematic approach demonstrated that combination immunotherapy rescued T cell dysfunction while promoting a memory phenotype and also revealed the molecular pathways driving durable antitumor responses in the MC38 and RENCA tumor models. Identification of these pathways provides a rational basis for optimizing existing combination immunotherapies and improving tumor responsiveness.

RESULTS

Anti–PD-1 and anti-GITR Ab combination therapy synergistically rejects established tumors and reinvigorates dysfunctional intratumoral CD8$^+$ T cells

To examine the antitumor effect of PD-1 and GITR combination immunotherapy, we first used a widely studied and poorly immunogenic murine MC38 colon adenocarcinoma model (Fig. 1A). Although variable reductions in tumor volume and modestly prolonged survival have been reported in this model (*10*), monotherapy with anti–PD-1 or anti-GITR [DTA-1 rat immunoglobulin G2b (IgG2b)] Ab is not effective at inducing complete and durable tumor regression

Regeneron Pharmaceuticals,Tarrytown, New York, NY 10591, USA.
*These authors contributed equally to this work.
†Corresponding author. Email: dimitris.skokos@regeneron.com

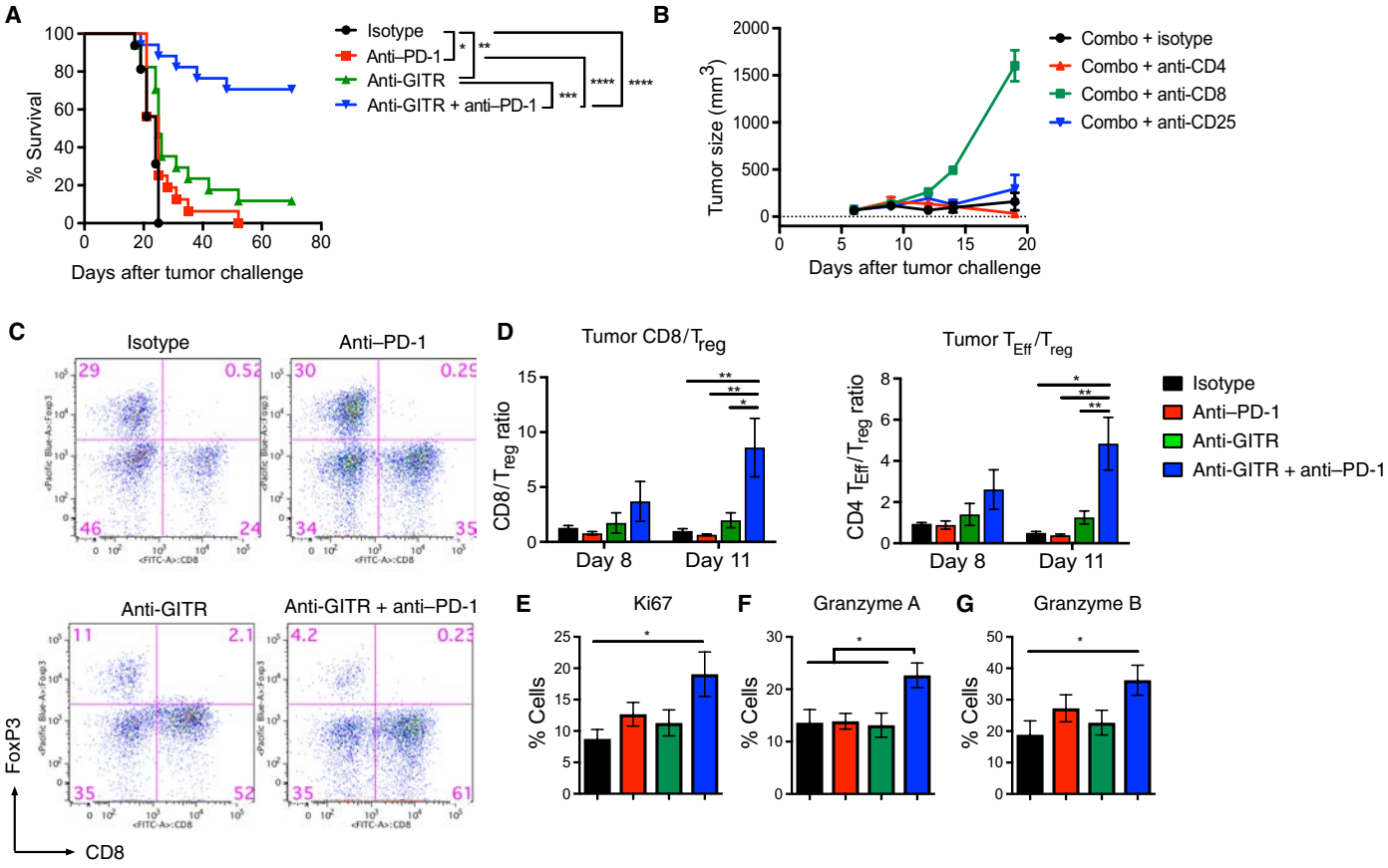

Fig. 1. Anti-GITR and anti–PD-1 combination synergistically rejects established murine tumors and reinvigorates intratumoral dysfunctional T cells. (**A**) Survival curve of MC38 tumor–bearing mice treated with anti-GITR and/or anti–PD-1 Ab treatment (days 6 and 13). Results depict cumulative survival curves with indicated treatment (n = 16 to 17 mice per group). (**B**) $CD8^+$ T cell–dependent long-term tumor protection mediated by combination treatment. C57BL/6 mice were treated with anti-CD8–, anti-CD4–, or anti-CD25–depleting Ab before and during therapy with anti-GITR and anti–PD-1 Ab or control Ab. Data shown are average tumor growth curve upon treatment with different depletion Abs (n = 6 mice per group). (**C** and **D**) Combination treatment increases intratumoral T_{Eff}/T_{reg} ratio. (C) Representative FACS plots showing tumor T cell subsets on day 11 ($FoxP3^+$ versus $CD8^+$, cells pregated on live/single cells/$CD45^+/CD3^+$). FITC, fluorescein isothiocyanate. (D) Summary FACS result of intratumoral $CD8^+$ T cell/T_{reg} and $CD4^+$ T_{Eff}/T_{reg} ratio on days 8 and 11 after tumor challenge. Data are representative of three independent experiments (n = 7 mice per group). (**E** to **G**) Combination treatment reinvigorates intratumoral dysfunctional T cells. Tumors were harvested on days 11 and 12 after implantation, dissociated into single-cell suspension restimulated with phorbol 12-myristate 13-acetate/ionomycin with the presence of brefeldin A. Cells were fixed and permeabilized, followed by intracellular staining with Ki67 (E), granzyme A (F), and granzyme B (G). Data shown are percentages of positive cells (n = 8 to 9 mice per group). All error bars in figures show SEM. *P < 0.05, **P < 0.01, ***P < 0.001, ****P < 0.0001, log-rank test (A) and one-way ANOVA with Tukey's test (C to G).

in established tumors (*8*, *11*, *12*). To determine the relative contribution of GITR agonism, we selected the DTA-1 mouse IgG2b isotype in this model to avoid maximum regulatory T cell (T_{reg}) depletion as seen with the mouse IgG2a isotype, allowing us to test the effect of the combination therapy. The Abs were administered on 6 and 13 days after tumor challenge when tumors were palpable. In line with previous studies (*9*, *12*, *13*), whereas anti-GITR or anti–PD-1 treatment alone exhibited little antitumor effect, combination therapy synergistically prolonged overall survival time of mice (~70% of mice were tumor free for >80 days; Fig. 1A). Cell depletion studies showed that tumor rejection was primarily dependent on the $CD8^+$ T cells, because removal of $CD8^+$ T cells abrogated the antitumor effect elicited by anti–PD-1/GITR Ab treatment (Fig. 1B and fig. S1). The antitumor effect was associated with a reduction in intratumoral T_{reg} and a robust increase in the effector $CD8^+$ and $CD4^+$ T cell (T_{Eff})–to-T_{reg} ratio, indicating a more immunostimulatory microenvironment (Fig. 1, C and D) and validating previous findings by other groups (*13*, *14*). In addition, combination therapy increased proliferation (as judged by expression of Ki67) and granzyme A and B production by intratumoral $CD8^+$ T cells (Fig. 1, E to G).

Concurrent single-cell TCR and transcriptome analyses identified a unique gene signature of clonally expanded $CD8^+$ T cells upon combination immunotherapy

We developed and validated a new bioinformatics platform designated rpsTCR (for random priming sequencing TCR) to extract, reconstruct, and analyze TCR sequences after single-agent or combination treatment. Briefly, this platform uses random priming RNA sequencing (RNA-seq) data generated from sorted single cells to identify mouse T cell clones potentially associated with tumor reactivity across different treatments (fig. S2 and table S2) (*15*). Mice were treated as described in Fig. 1, and more than 2000 $CD8^+$ T cells were sorted from tumor-bearing mice at days 8 and 11 after tumor challenge (Fig. 2A). The rpsTCR platform was used to profile the TCR sequences of 1379

$CD8^+$ T cells. Our detection rates of TCRB-CDR3 (86%), TCRA-CDR3 (78.2%), and paired TCRB and TCRA (73.1%) were comparable with the reported detection rates using targeted TCR sequencing from single T cells (table S2) (*15*). At the early time point (day 8), very few clones of high-frequency T cells (defined as ≥ 3 T cells sharing identical TCR sequences) were detected in all treatment groups (fig. S3). By day 11, we identified two high-frequency T cell clones (representing 5.7% of sequenced single $CD8^+$ T cells) from isotype control samples—3 clones (20.3%) for anti-GITR samples and 6 clones (26.7%) for anti–PD-1 samples—and 10 clones (31.9%) for combination-treated samples. Between days 8 and 11, a significant clonal expansion of intratumoral $CD8^+$ T cells was induced by anti–PD-1 monotherapy, in agreement with published data on human melanoma patients (*16*) showing an increase in TCR clonal size after anti–PD-1 therapy with pembrolizumab. Our results extend these findings by showing that dual targeting of PD-1 and GITR further enhances intratumoral $CD8^+$ T cell TCR clonal expansion (fig. S3). Of note, anti-GITR and/or anti–PD-1 had no significant impact on peripheral (spleen) T cell clonality (fig. S3), consistent with patient data using pembrolizumab (*16*).

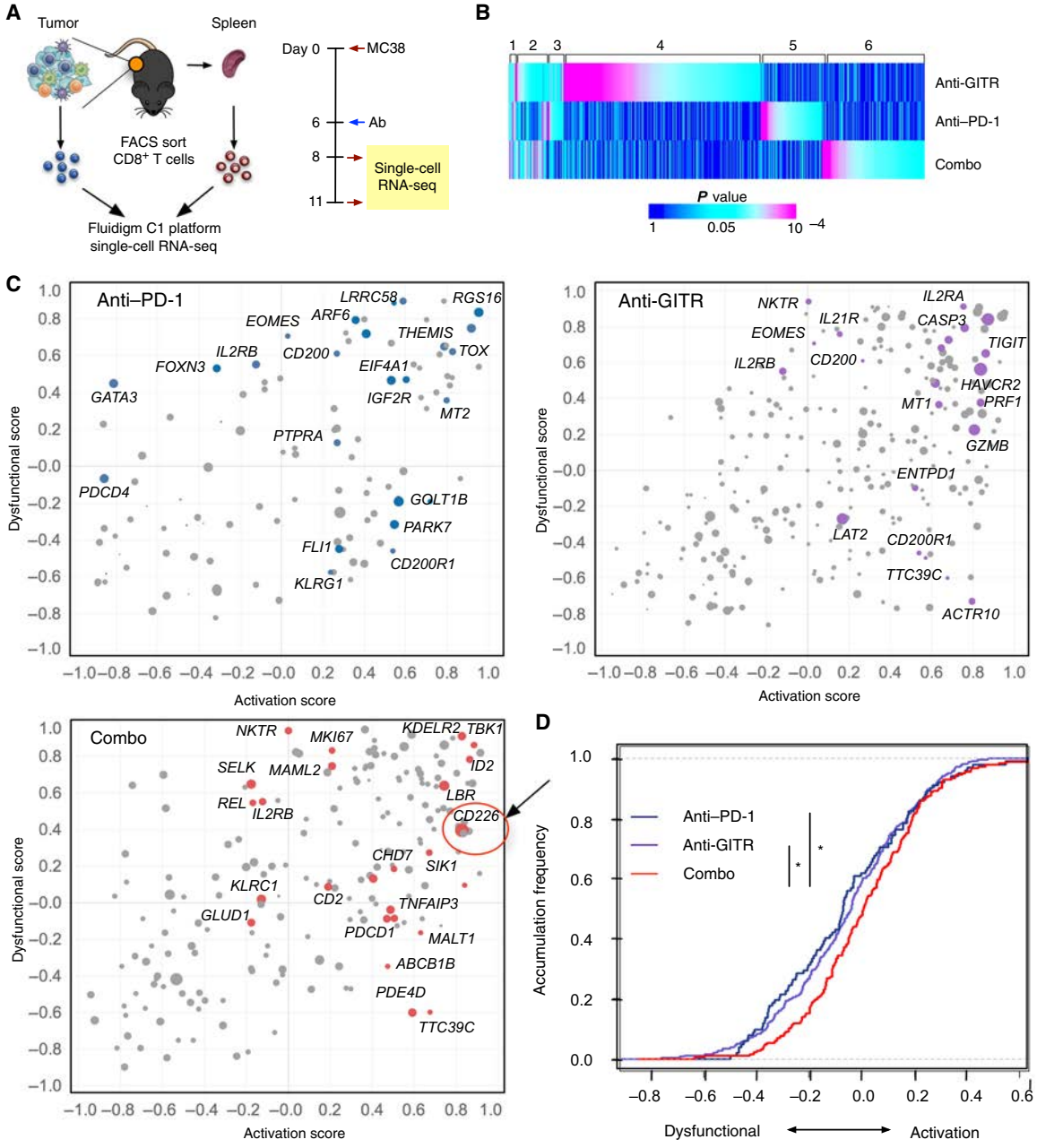

Fig. 2. Single-cell RNA-seq analysis of intratumoral $CD8^+$ T cells reveals unique gene profiles upon combination treatment. (**A**) Schematic of tumor immunotherapy and single-cell sorting study design. (**B**) Heat map of significantly changed genes in clonal expanded intratumoral $CD8^+$ T cells upon different treatment. Numbers indicate unique gene clusters (see table S3 for gene list). Color gradient indicates the *P* value. (**C**) Distribution of genes significantly affected by each treatment on the dysfunctional/activation plot. (**D**) KS plot of the values of the gene signatures on the dysfunction ↔ activation axis (KS, $P < 0.05$).

To evaluate the effect of combination therapy on the activation state of intratumoral CD8$^+$ T cells, we performed gene expression pathway analysis on clonally expanded CD8$^+$ T cells. Combination treatment synergistically integrated the pathways modulated by each single agent, resulting in a distinct transcriptional state associated with induction of adaptive immune response, cell cycle, and metabolic activity gene expression pathways (Table 1). We then applied to our data the uncoupled T cell dysfunction and activation gene expression module analysis, as described by Singer *et al.* (*17*). A total of 452 genes were significantly regulated by either single-agent or combination treatment compared with isotype control. These genes were plotted against the activation/dysfunctional score (Fig. 2B, $P < 0.05$). Genes shared or unique across treatment groups were sorted on the basis of *P* value and then grouped into six clusters (Fig. 2C). Selected genes differentially increased in each group and fold changes compared with isotype control treatment are listed in table S3. Up-regulation of certain T cell activation markers (i.e., *IL2rb*) was shared across treatment groups, whereas most of the differentially regulated gene signatures were nonoverlapping, consistent with distinct transcriptional states of expanded CD8$^+$ T cell clones. GITR agonism specifically up-regulated genes involved in T cell activation/cytotoxicity (*Il2ra*, *Txk*, *Gzme*, *Gzmd*, and *Prf1*), in prosurvival function (*Tnfrsf1b*), and in immune checkpoint (*Havcr2*, *Tigit*, and *Entpd1*). PD-1 blockade stimulated induction of *Gata3*, *Tox*, *Mt2*, and *Pdcd4* (*18*), which are involved in T cell dysfunction and apoptosis, and promoted expression of *Themis* assisting TCR signaling to low-affinity ligands (*19*). *Cd226*, a costimulatory molecule that plays an important role in antitumor response (*20*), was the most up-regulated gene upon combination therapy, followed by other genes involved in signal transduction and T cell differentiation/activation (*Pde4d*, *Vav1*, *Mki67*, and *Id2*) (*21*–*23*). Furthermore, combination treatment, in contrast to monotherapy, selectively prevented the up-regulation of genes involved in T cell differentiation/dysfunction, such as *Eomes*, *Mt1*, *Mt2*, and *Cd200*.

Table 1. Pathways specifically up-regulated in clonal expanded CD8$^+$ T cells with Ab treatment (day 11). Genes specifically up-regulated in monotherapy or combination therapy compared with isotype control were analyzed using Illumina Gene Ontology Engine. Jak, Janus kinase; STAT, signal transducers and activators of transcription.

Treatment	Pathway	*P* value
Anti–PD-1 + Anti-GITR	Adaptive immune response	1.50×10^{-08}
	Cell cycle	5.80×10^{-07}
	Metabolism of lipids and lipoproteins	3.00×10^{-04}
Anti–PD-1	Lymphocyte activation	2.30×10^{-05}
	Gene targets for miR-124u (T cell activation)	1.80×10^{-05}
	Jak-STAT signaling pathway	3.00×10^{-04}
Anti-GITR	Glucose metabolism	8.20×10^{-10}
	Protein metabolism	7.50×10^{-08}
	The citric acid cycle and respiratory electron transport	3.90×10^{-06}

This activation and dysfunctional module score allowed us to quantitatively compare the complex T cell activation profile among different treatment groups. The activation module had significantly higher scores in the combination versus monotherapy treatment groups, indicative of a more activated T cell state [Fig. 2D; Kolmogorov-Smirnov (KS) test, $P < 0.05$].

Overall, although single-agent therapy expanded intratumoral CD8$^+$ T cell clones and modulated critical gene pathways, this was not sufficient for complete and long-lasting tumor rejection (Fig. 1A). Our findings suggest that a profound reprogramming of dysfunctional tumor-infiltrating T cells by combination therapy was required for tumor rejection and long-term response. This result is supported by a recent study showing that CD8$^+$ T cells quickly become dysfunctional at early stage of tumor development and gradually evolve into a less flexible state (*24*).

Anti–PD-1 and anti-GITR combination therapy modulates distinct tumor-specific CD8$^+$ T cell populations

To determine whether distinct cellular mechanisms underlie anti–PD-1– and anti-GITR–mediated tumor rejection, we profiled tumor-infiltrating T cells by high-dimensional flow cytometry and used well-validated data-driven unsupervised clustering approaches (*25*, *26*). Our attempt to use published mutated MC38 tumor epitopes (*27*) to track MC38-specific T cell clones was not successful. This possibly reflects the different mutation status of tumor cell lines between laboratories, likely due to intrinsic genome instability of the tumor cells (*28*). As an alternative approach, we generated MC38 tumor cell variant expressing H-2K^b single-chain trimer of major histocompatibility complex class I with SIINFEKL peptide (as a surrogate tumor epitope) and β_2m [ovalbumin (OVA)–β_2m-K^b; fig. S4A]. This allowed us to track Ag (OVA/SIINFEKL)–specific CD8$^+$ T cells, which can be identified by H-2K^b–SIINFEKL pentamer staining (fig. S4B). Consistent with the TCR clonality analysis (fig. S3), anti–PD-1 Ab and combination treatment induced significant clonal expansion of OVA-specific CD8$^+$ T cells intratumorally. Only the combination therapy significantly increased the intratumoral density (cell number normalized to milligrams of tumor tissue). A fluorescence-activated cell sorter (FACS)–based method was used, which allowed us to sample substantially more cells than the capacity of single-cell RNA-seq; thus, we were able to identify significant clonal expansion induced by combination therapy in spleen (fig. S4B). Functionally, clonally expanded OVA-specific T cells produced higher levels of interferon-γ (IFN-γ) upon OVA peptide restimulation (fig. S4C).

Next, we profiled T cells from tumor-bearing mice treated with anti-GITR and/or anti–PD-1 Ab using T cell differentiation/activation markers (e.g., PD-1, TIM3, LAG3, KLRG1, CD244, and CD44) and T cell lineage transcription factors (e.g., Eomes and Tbet). We detected heterogeneity within the Ag-specific CD8$^+$ T cells, reflecting different activation/differentiation states (Fig. 3A). At day 9, T cell populations between treatment groups were indistinguishable; however, a marked skew in the population was observed by day 12 in response to anti-GITR Ab alone or combination treatment (Fig. 3B). To gain a more comprehensive understanding of the phenotypes of the T cell populations that were affected by the treatment, we analyzed Ag-specific CD8$^+$ T cells using unsupervised spanning-tree progression analysis of density-normalized events (SPADE) clustering. Fourteen distinct Ag-specific CD8 T cell clusters (>2% relative frequency) were identified (Fig. 3C). Among them, clusters 14, 12, and 7 were highly responsive to anti-GITR and anti–PD-1 treatment (Fig. 3D). On the basis of the high expression level of T cell activation/dysfunction markers (PD-1,

TIM3, LAG3, CD244, Eomes, Tbet, and KLRG1), these three clusters likely represent different stages of dysfunction (Fig. 3E and fig. S5), unlike cluster 10 representing a more naïve/quiescent phenotype. Cluster 14 is absent at the earlier time point and has the highest expression level of markers associated with dysfunctional T cells, suggesting a terminal stage of dysfunction. All treatment groups were associated with a relative decrease in dysfunctional T cell frequency, and there was no significant difference between treatment groups (Fig. 3D). To evaluate the dysfunctional state (plastic versus nonprogrammable) (*24*), we examined the expression level of PD-1, LAG3, CD38, CD101, and CD5 on intratumoral Ag-specific T cells. Using an unsupervised hierarchical clustering algorithm [cluster identification, characterization, and regression (CITRUS), Cytobank], we found that combination and anti-GITR Ab treatment significantly decreased a T cell cluster with a profile matching the nonprogrammable dysfunctional T cells (PD-1^{hi}LAG3^{hi}CD38^{hi}CD101^{hi}CD5^{low}; Fig. 3, F and G).

To further characterize the responsive T cell populations, we used additional differentiation and activation markers to phenotypically dissect the T cells (e.g., Sca1, CD95, CD127, CD122, CD226, and Ki67). Unique cell populations can be identified upon treatment on day 12 (Fig. 4, A and B, and fig. S6). SPADE clustering was conducted using this specific panel of markers (Fig. 4C) to allow for statistical analysis between groups for a single cluster. We observed a specific effect of the combination treatment that was driven primarily by the anti-GITR Ab in expanding a unique memory cell population (cluster 11; Fig. 4, C to F) that may confer long-lasting protective immunity. These cells express CD62L and CD44 (Fig. 4E), similar to memory cells in the spleen compartment, while up-regulating additional key markers (Sca1, CD95, CD127, CD122, and Eomes), characteristic of a memory precursor effector cell phenotype (MPEC) as previously described (*29*) (Fig. 4F). Overall, combination therapy drives the expansion of MPECs, which represent a very small fraction of CD8$^+$ T_{Effs} expressing CD127/IL7R. MPECs have high propensity to survive

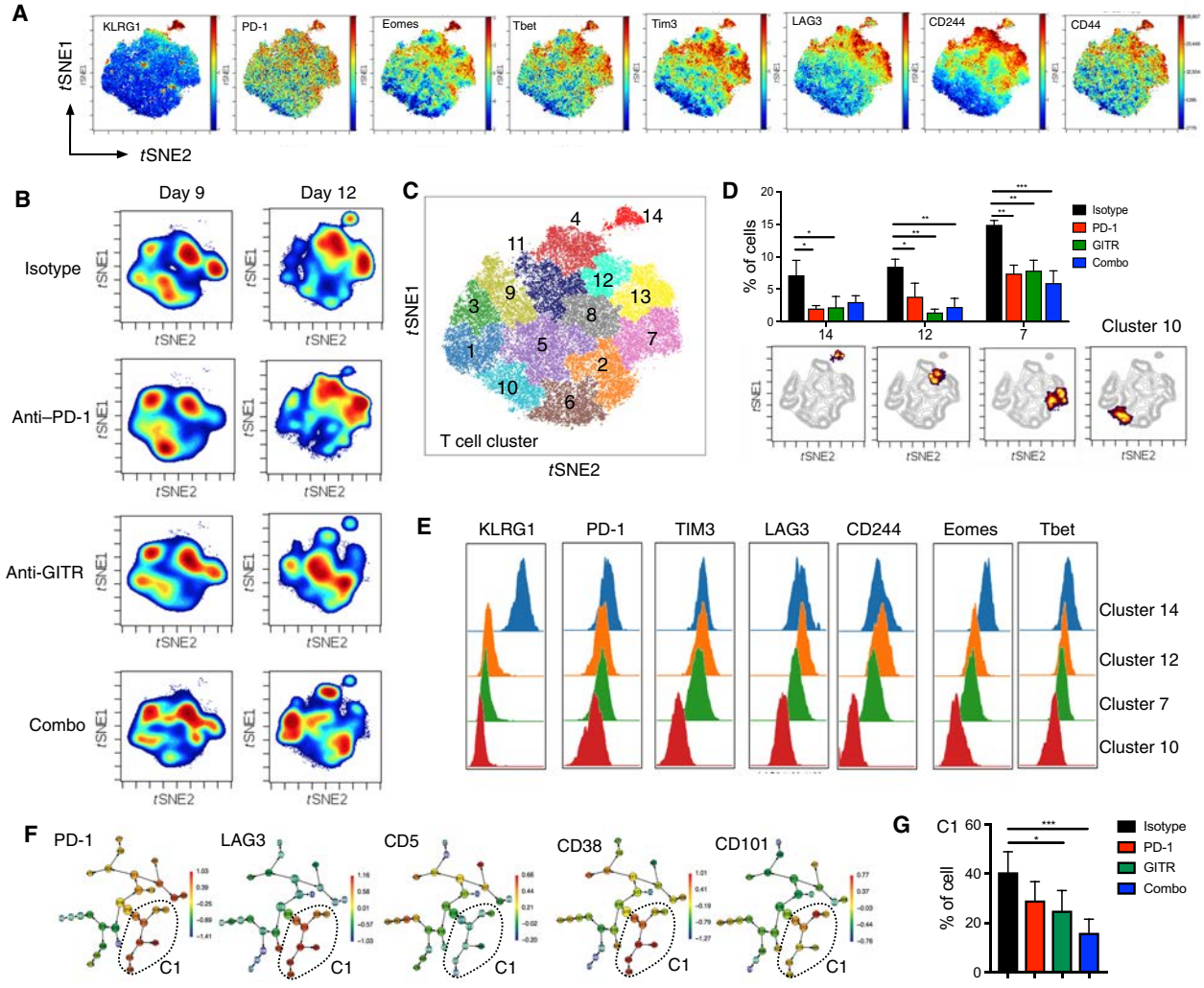

Fig. 3. Identification of combination treatment–responsive dysfunctional tumor-infiltrating CD8$^+$ T cell population. (**A**) Density viSNE plots of OVA-specific intratumoral CD8$^+$ T cells from each treatment group days 9 and 12 after tumor challenge. (**B**) viSNE plots of tumor-infiltrating T cells overlaid with the expression of indicated markers. (**C**) viSNE plot of intratumoral OVA-specific CD8$^+$ T cells overlaid with color-coded T cell clusters identified by SPADE. (**D**) Frequency of selected T cell clusters displayed on a per-mouse basis with means ± SEM. Indicated cluster was highlighted on viSNE plot below the bar graph. (**E**) Histogram displaying the expression level of indicated markers on T cell clusters. (**F**) CITRUS cluster result overlaid with indicated markers. Cluster that was significantly affected with Ab treatment is circled (C1). (**G**) Frequency of cluster C1 is shown with means ± SEM. *P < 0.05, **P < 0.01, ***P < 0.001, one-way ANOVA test.

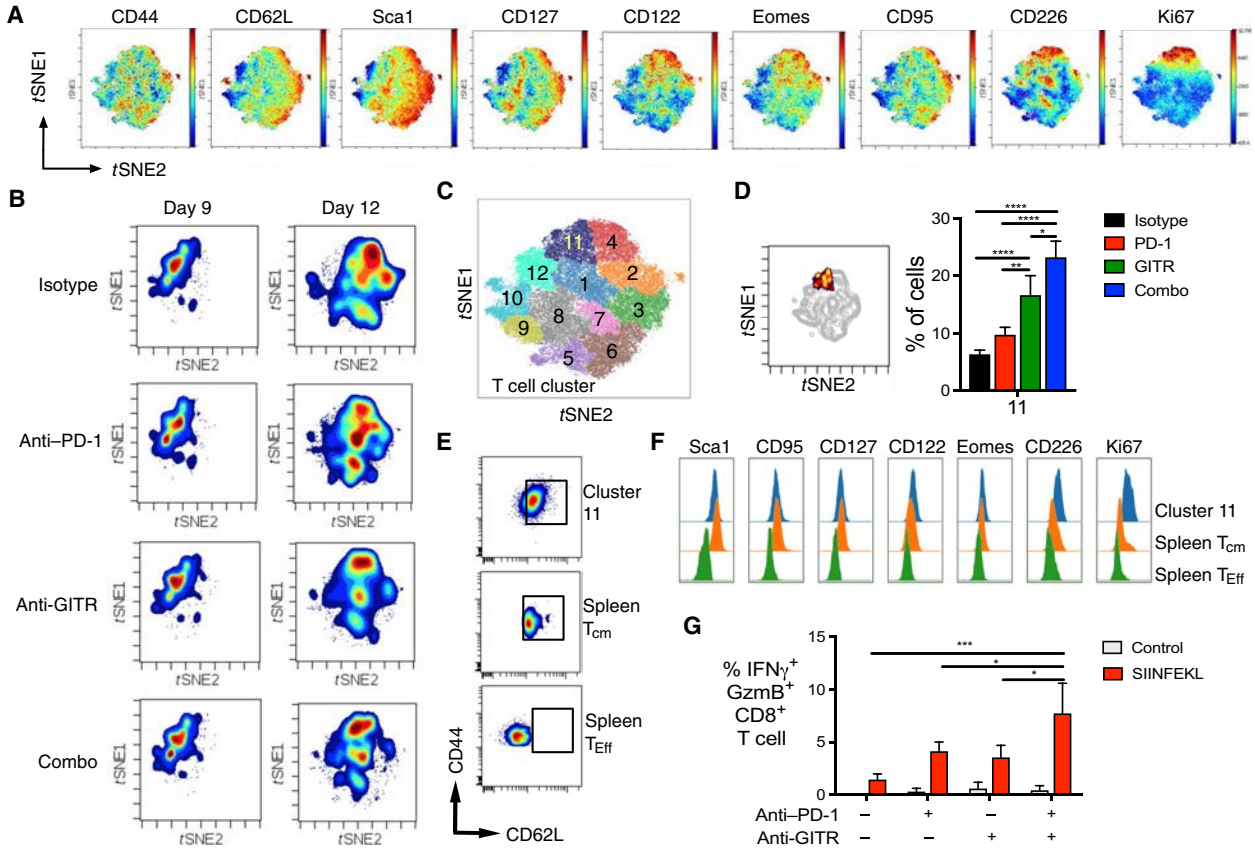

Fig. 4. Identification of combination treatment–responsive effector/memory tumor-infiltrating CD8$^+$ T cell population. (**A**) viSNE plots of tumor-infiltrating T cells overlaid with the expression of selected markers. (**B**) Density viSNE plots of OVA-specific tumor-infiltrating CD8$^+$ T cells from each treatment group days 9 and 12 after tumor challenge. (**C**) viSNE plot of MC38 infiltrating OVA-specific CD8$^+$ T cells overlaid with color-coded T cell clusters identified by SPADE. (**D**) Frequency of selected T cell clusters (means ± SEM). Indicated cluster was highlighted on viSNE plot below the bar graph. (**E**) FACS plots of CD44 and CD62L expression on cluster 11 compared with spleen T cell subsets. T_{cm} central memory T cells. (**F**) Histogram displaying the expression level of selected markers on T cell clusters. (**G**) Frequency of cytokine production of CD8$^+$ T cells upon restimulation in vitro with OVA peptide. GzmB, granzyme B. *$P < 0.05$, **$P < 0.01$, ***$P < 0.001$, ****$P < 0.0001$, one-way ANOVA with Tukey's test).

and become functional memory T cells, which are essential to confer protective immunity (*3*). These cells also express high levels of CD226 and Ki67, suggesting an activated and highly proliferative state (Fig. 4F). Further, these intratumoral OVA-specific CD8$^+$ T cells from cluster 11 showed increased IFN-γ, and granzyme B production upon Ag-specific restimulation followed single-agent treatment, but only combination treatment significantly enhanced their function (Fig. 4G).

In agreement with previous findings, we showed that although anti–PD-1 alone induces a less dysfunctional tumor-infiltrating lymphocyte (TIL) phenotype (Fig. 3), it is associated with low T_{EMs} (*30*, *31*) and lack of long-term survival (Fig. 1) (*32*). We demonstrated that combination therapy can promote a memory CD8$^+$ T cell phenotype, indicating that a costimulatory agonist Ab can synergize with PD-1 checkpoint blockade, leading to long-term antitumor responses. We further investigated the mechanism by which this specific combination therapy effect occurred by functional analysis of the identified up-regulated genes.

CD226 expression is induced on tumor-specific CD8$^+$ T cells upon combination therapy

CD226, a costimulatory molecule with a well-validated role in the development of antitumoral immune response (*31*), was identified as the most up-regulated gene upon combination therapy (Fig. 1, B and C, and table S3). We performed a *Cd226* expression analysis on different subsets of intratumoral CD8$^+$ T cells (total, clonally expanded, or nonexpanded) across treatment groups (Fig. 5A), which revealed that *Cd226* mRNA levels were significantly increased by combination treatment on clonally expanded T cells (fold change, 10.7), whereas this difference was diluted in bulk/total CD8$^+$ T cells (fold change, 3.5) and nonexpanded CD8$^+$ T cells (not significant). Further, *Cd226* mRNA levels were significantly increased by combination treatment on clonally expanded CD8$^+$ T cells in comparison to anti–PD-1 (fold change, 6.5) and anti-GITR (fold change, 9.2). Using the MC38-OVA-β_2m-K^b model, we found that protein levels of CD226 were highest on spleen OVA-specific CD8$^+$ T cells after anti–PD-1 treatment (Fig. 5B) and were further elevated by combination treatment. The same treatment had no significant effect on the CD226 levels of nonspecific CD8$^+$ T cells. This dataset suggests that anti–PD-1 treatment could play a dominant role in driving the increase of CD226 on Ag-specific T cells, providing key information on the mode of action of anti–PD-1 in antitumor immunity.

CD226 is a substrate for dephosphorylation by PD-1–SHP2

Next, we investigated a potential association between PD-1 signaling and CD226. The costimulatory receptor CD28 was previously identified as a target for PD-1–SHP2 dephosphorylation (*32*). Experiments using a cell-free reconstitution system in which the cytoplasmic domain

of PD-1 was bound to the surface of large unilamellar vesicles (LUVs) that mimic the plasma membrane of T cells demonstrated that CD28 is preferred over the TCR as a target for SHP2-mediated dephosphorylation. Using the same system, we examined whether CD226 could be another target for dephosphorylation by the PD-1–SHP2 complex. We reconstituted different components (CD3, CD226, etc.) involved in T cell signaling on the liposomes (Fig. 5C) (*33*). The sensitivity of each component in response to PD-1 titration on the LUVs was measured by phosphotyrosine (pY) Western blots. We confirmed previous published data (*32*) showing that CD28, but not inducible T cell costimulator (ICOS), is a substrate for desphosphorylation by PD-1–SHP2 (Fig. 5D). We found that CD226 was efficiently dephosphorylated by PD-1–SHP2 in a dose-dependent manner (Fig. 5D) in the presence of LFA-1. Although LFA-1 facilitates T cell activation by lowering the amounts of antigen necessary for T cell activation (*33*), cross-linking of LFA-1 induces tyrosine phosphorylation of DNAM-1 (CD226) (*34*). Although additional experiments are needed to fully characterize the basis of CD226 sensitivity to PD-1–SHP2–induced dephosphorylation, we demonstrated a biochemical association between PD-1 signaling and CD226 dephosphorylation using a cell-free biochemical system. To validate these findings in a more physiologically relevant system involving primary cells from the tumor microenvironment, we isolated Ag-specific intratumoral CD8$^+$ T cells from MC38-OVA tumor–bearing mice (day 11) previously treated with anti–PD-1 Ab or isotype control Ab. Consistent with the cell-free in vitro assay, we found that CD8$^+$ TILs from the PD-1 Ab–treated group showed high CD226

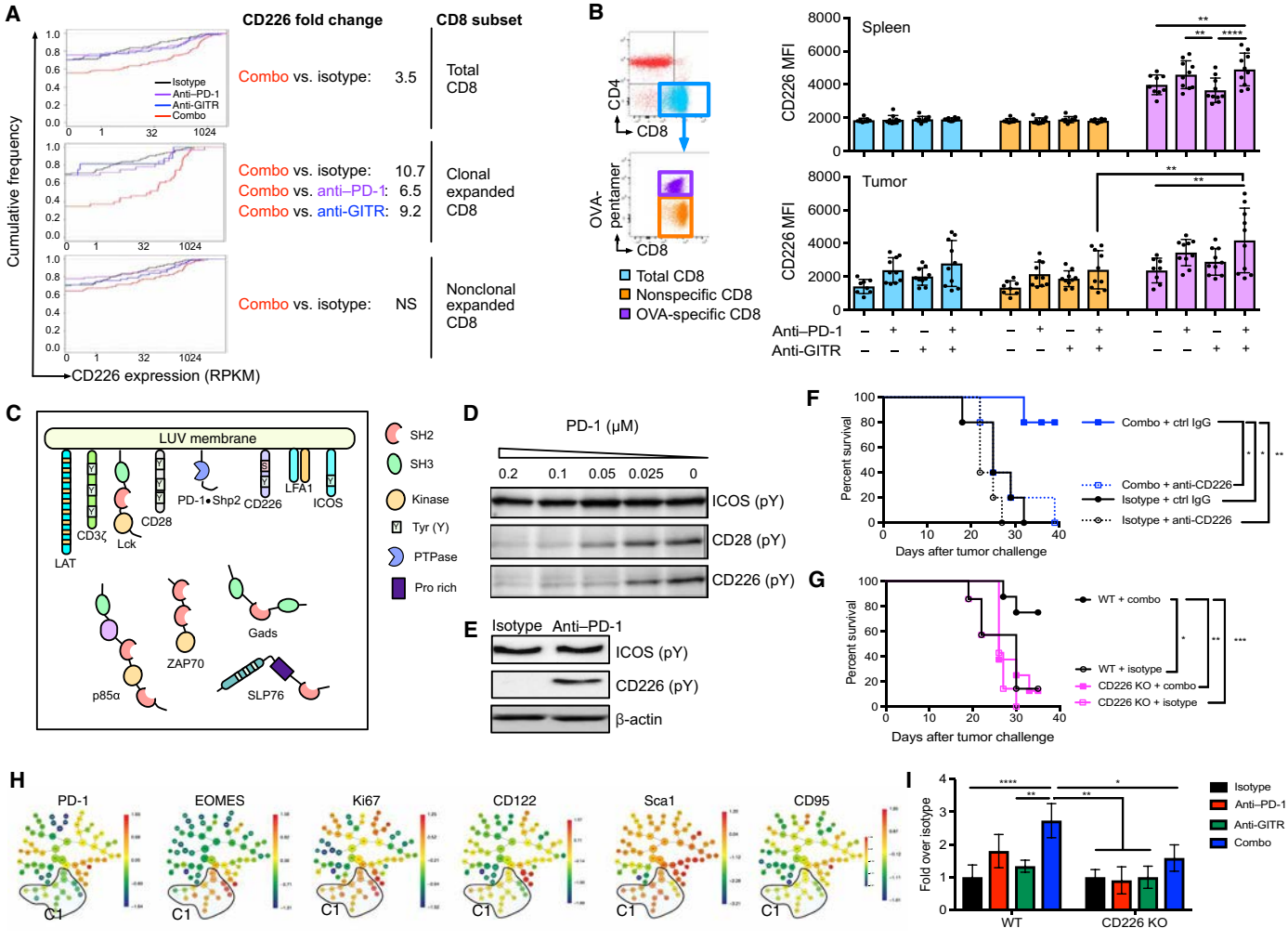

Fig. 5. CD226 signaling pathway is essential in mediating antitumor response induced by combination treatment in MC38 tumor model. (**A**) Cumulative distribution function plots show the expression of *CD226* in total, clonal expanded, or nonexpanded CD8$^+$ T cells. Fold changes of *CD226* expression level are indicated for each subset. RPKM, reads per kilobase million. (**B**) FACS analysis of CD226 expression [mean fluorescence intensity (MFI)] on spleen/tumor CD8$^+$ T cell populations, gating strategy indicated in FACS plots. Data show one representative experiment of two independent experiments (n = 10 mice per group). (**C**) Schematic shows LUVs. (**D**) Western blot shows phosphorylation status of ICOS, CD28, and CD226 with increasing PD-1 concentrations. (**E**) Western blot shows phosphorylation status of ICOS and CD226 from intratumoral OVA-specific CD8$^+$ T cells purified from mice treated with isotype or anti–PD-1 Ab. (**F**) MC38 tumor–bearing mice were treated with CD226-blocking Ab or isotype IgG before immunotherapy with anti-GITR and anti–PD-1 or isotype IgGs. The percentages of survival are shown here. Data show one representative experiment of three independent experiments (n = 5 mice per group). (**G**) CD226 KO mice or WT littermates were challenged with MC38 tumor cells and treated with either anti-GITR and anti–PD-1 Ab or isotype Abs on days 6 and 13 after tumor implantation. Data show one representative experiment of two independent experiments (n = 7 to 8 mice per group). (**H**) CITRUS cluster result overlaid with indicated markers. Cluster C1 that was significantly affected with Ab treatment is circled. (**I**) Frequency of T cell cluster C1 displayed on a per-mouse basis with means ± SEM. *P < 0.05, **P < 0.01, ***P < 0.001, ****P < 0.0001, one-way ANOVA with Tukey's test.

phosphorylation upon PD-1 inhibition (Fig. 5E), confirming that CD226 is in an activated state. $CD8^+$ TILs from isotype control–treated mice showed a lack of CD226 phosphorylation, indicating that PD-1/PD-L1 pathway is a negative regulator of CD226 activity on intratumoral $CD8^+$ T cells. These data suggest that CD226 is an additional substrate for dephosphorylation by PD-1–SHP2.

Down-regulation of TIGIT expression upon GITR Ab treatment shifts the CD226/TIGIT pathway toward stronger costimulation

It has recently been shown that the strength of $CD8^+$ T cell response is affected by the overall balance between CD226 and the coinhibitory receptor TIGIT (*31*). Single-cell RNA-seq data indicated that anti-GITR Ab treatment increased TIGIT transcripts in high-frequency T cell clones (fig. S7A), whereas FACS analysis showed lower expression of TIGIT on OVA-specific $CD8^+$ T cells with anti-GITR or combination treatment compared with anti–PD-1 treatment alone (fig. S7B). This result is consistent with the observation that TIGIT expression is tightly regulated at the posttranscriptional level (*35*). Combination treatment significantly decreased the percentage of $TIGIT^+$ cells and the expression level on a per-cell basis on total tumor-infiltrating $CD8^+$ and $CD4^+$ T_{Effs} and T_{regs}, the effect of which was mainly driven by anti-GITR Ab treatment (fig. S7, C and D). Combination and/or monotherapy treatment had no effect on the percentage of $CD226^+$ tumor-infiltrating $CD4^+$ T cells, splenic $CD4^+$ T cells, or splenic T_{regs} (fig. S7E). TIGIT expression level (fig. S7F) on the dysfunctional T cell cluster 14 (identified in Fig. 3D) is uniformly high (~100%), whereas the memory-like T cell cluster 11 (identified in Fig. 4D) shows much lower levels of TIGIT expression.

In addition, because GITR is highly expressed on T_{regs}, we performed a comprehensive profiling [*t*-distributed stochastic neighbor embedding (t-SNE)–based visualization (viSNE)/SPADE] analysis on the remaining intratumoral T_{regs} upon combination treatment and compared the results to a well-studied T_{reg}-depleting Ab (anti-CD25, PC61). We found that GITR and PD-1 combination therapy has a distinct effect on the phenotype of the remaining T_{regs} compared with the anti-CD25 Ab treatment group. GITR and PD-1 combination treatment skewed the remaining T_{reg} subsets toward a less suppressive phenotype, as defined by a lower expression of TIGIT, KLRG1, LAG3, and TIM3 (fig. S8). All these markers have been reported to identify a highly activated and phenotypically suppressive T_{reg} population (*36*, *37*). To assess whether the distinct effect of GITR and CD25 Abs on T_{reg} depletion could differentially alter the phenotype of $CD8^+$ T cells, we analyzed the intratumoral OVA-specific $CD8^+$ T cells (fig. S9). Using an extended 18-parameter viSNE analysis, we found that GITR and PD-1, but not CD25 and PD-1, combination Ab treatment significantly decreased the dysfunctional phenotype (cluster 1: low Ki67, CD226, Sca1, CD95, CD122, high KLRG1, PD-1, LAG3, and CD244) and the naïve-like T cells (cluster 10: $CD62L^+CD44^-$, low Ki67, CD226, PD-1, and other T cell activation markers), whereas it increased the cluster with memory-like activated T cell phenotype (cluster 6: high CD226, Ki67, Sca1, CD127, CD95, and CD122 and lower level of PD-1, TIM3, LAG3, KLRG1, and CD244). These data show that the shift in balance between CD226 and TIGIT is driven by the direct combination of PD-1 and GITR Abs and not solely through a reduction in intratumoral T_{regs} (fig. S9, E and F).

Overall, the single-cell RNA-seq and FACS phenotyping data showed that anti–PD-1 favored the increased expression of CD226, whereas anti-GITR treatment down-regulated surface expression of TIGIT and reduced intratumoral T_{reg} subsets with a highly suppressive phenotype, therefore synergistically restoring the homeostatic $CD8^+$ T cell function.

CD226 signaling pathway is essential in mediating the antitumor response induced by combination treatment

Using a CD226-blocking monoclonal Ab, we showed that costimulatory signaling through CD226 is required for the antitumor immunity mediated by combination treatment (Fig. 5F). To validate the T cell intrinsic role of CD226, we genetically inactivated it in C57BL/6 background mice (fig. S10, A and B). CD226 knockout (KO) mice showed no defect on T cell ($CD4^+$, $CD8^+$, and T_{regs}) development and homeostasis (fig. S10, C and E) or responsiveness to TCR activation when compared with wild-type (WT) littermates (fig. S10F). After tumor challenge in the CD226 KO mice, we found that combination treatment with anti–PD-1 and anti-GITR no longer conferred any antitumor effect or survival benefit, suggesting that CD226 is essential for the antitumor effect of the combination therapy (Fig. 5G). In addition, we validated the specificity of the CD226 pathway mediating this effect because inhibition of TNFR superfamily pathways (OX40/OX40L or 4-1BB/4-1BBL) or blockade of the B7 costimulatory molecule (CD28) with CTLA4-Ig had no impact on the antitumor effect observed with the combination treatment (fig. S11, A to C). In mice lacking CD226, combination therapy can no longer maintain the activated and highly proliferative memory T cell phenotype ($PD\text{-}1^{+/-}$, $Eomes^+$, $Ki67^+$, $CD122^+$, $Sca1^+$, and $CD95^+$), as observed in WT control tumor-bearing mice (Fig. 5, H and I).

To test whether the mechanisms found in the MC38 model also extend to other tumor cell models, we evaluated the role of PD-1 and GITR combination therapy in the RENCA tumor model (murine kidney carcinoma tumor in Balb/c background). This tumor cell line was chosen because it also showed relatively good expression of CD155, the endogenous ligand for CD226 (fig. S12). Consistent with the MC38 studies, anti-GITR and anti–PD-1 combination therapy can synergize and promote long-term survival of RENCA tumor–bearing mice (Fig. 6A). FACS analysis of tumor-infiltrating T cells revealed a significant reduction in T_{reg} driven by GITR Ab and expansion of tumor-specific $CD8^+$ T cells ($gp70\text{-}tetramer^+$) driven primarily by PD-1 Ab (Fig. 6, B and C). In addition, we also observed a significant increase of CD226 expression on tumor-specific $CD8^+$ T cells (Fig. 6D, gp70 $tetramer^+$ cells), consistent with our observations in the MC38 tumor model. viSNE and SPADE analyses (Fig. 6, E to G) revealed an increase in memory-like effector cell cluster (Fig. 6G, C5; high CD95, CD122, Ki67, and Tbet and low CD44 and TIM3) accompanied by reduced dysfunctional T cell cluster (Fig. 6G, C1; high TIM3 and low Ki67, CD95, CD122, Tbet, and Sca1). Likewise, when CD226 signaling is blocked by an anti-CD226 Ab during combination treatment, the antitumor efficacy is completely abrogated (Fig. 6I), as previously demonstrated in the MC38 tumor model. Thus, our data provide additional evidence that the role of CD226 is not limited to one tumor model or mouse genetic background.

DISCUSSION

We systematically profiled tumor-infiltrating $CD8^+$ T cells using single-cell TCR sequencing, transcriptomics, and high-dimensional flow cytometry clustering analysis to unveil the molecular mechanisms driving the potent synergism of a costimulatory agonist,

anti-GITR Ab, and a coinhibitory antagonist, anti–PD-1 Ab. We showed that a combination of these Abs synergistically enhanced the effector function of expanded $CD8^+$ T cells by restoring the balance of two key homeostatic regulators, CD226 and TIGIT, resulting in robust survival benefit.

Recently, it has been shown that T cell dysfunction represents an important hurdle for the generation of durable responses upon PD-1 inhibition (*3*). PD-1 blockade induces an incomplete rescue of T_{Ex}, thus failing to restore T_{Ex} into T_{EM}, a necessary requirement for effective immune memory (*38*, *39*). We demonstrated that combination therapy not only decreased the intratumoral $CD8^+$ T cells with a nonprogrammable dysfunctional profile (Fig. 3, F and G) (*31*, *40*) but also induced a highly proliferative TEM precursor population (Fig. 4) (*32*, *41*), thus eliciting potent antitumor immunity in a CD226-dependent manner (Figs. 5, F and G, and 6I). The similarity in the efficacy between both MC38 and RENCA tumor models despite different mouse genetic backgrounds and tumor types (C57BL/6 and Balb/c; colon and kidney adenocarcinoma, respectively) suggests that this mechanism is not limited to a specific tumor model. However, further research is needed to determine whether the reduction of dysfunctional $CD8^+$ T cells is through the reinvigoration of these populations and/or epigenetic reprogramming of them into a functional state (*24*).

Furthermore, we validated our findings using gene pathway analysis to show that although anti-GITR and anti–PD-1 monotherapies regulated distinct molecular pathways, combination treatment synergistically integrated the pathways modulated by each single agent, resulting in a distinct transcriptional state of $CD8^+$ T cells (Table 1). In addition, applying to our data the uncoupled T cell dysfunction and activation gene expression module score, as described by Singer *et al.* (*17*), enabled us to quantitatively compare the complex T cell activation profile between different treatment groups. We found that the activation module had significantly higher scores in the combination versus monotherapy treatments groups, indicative of a more activated

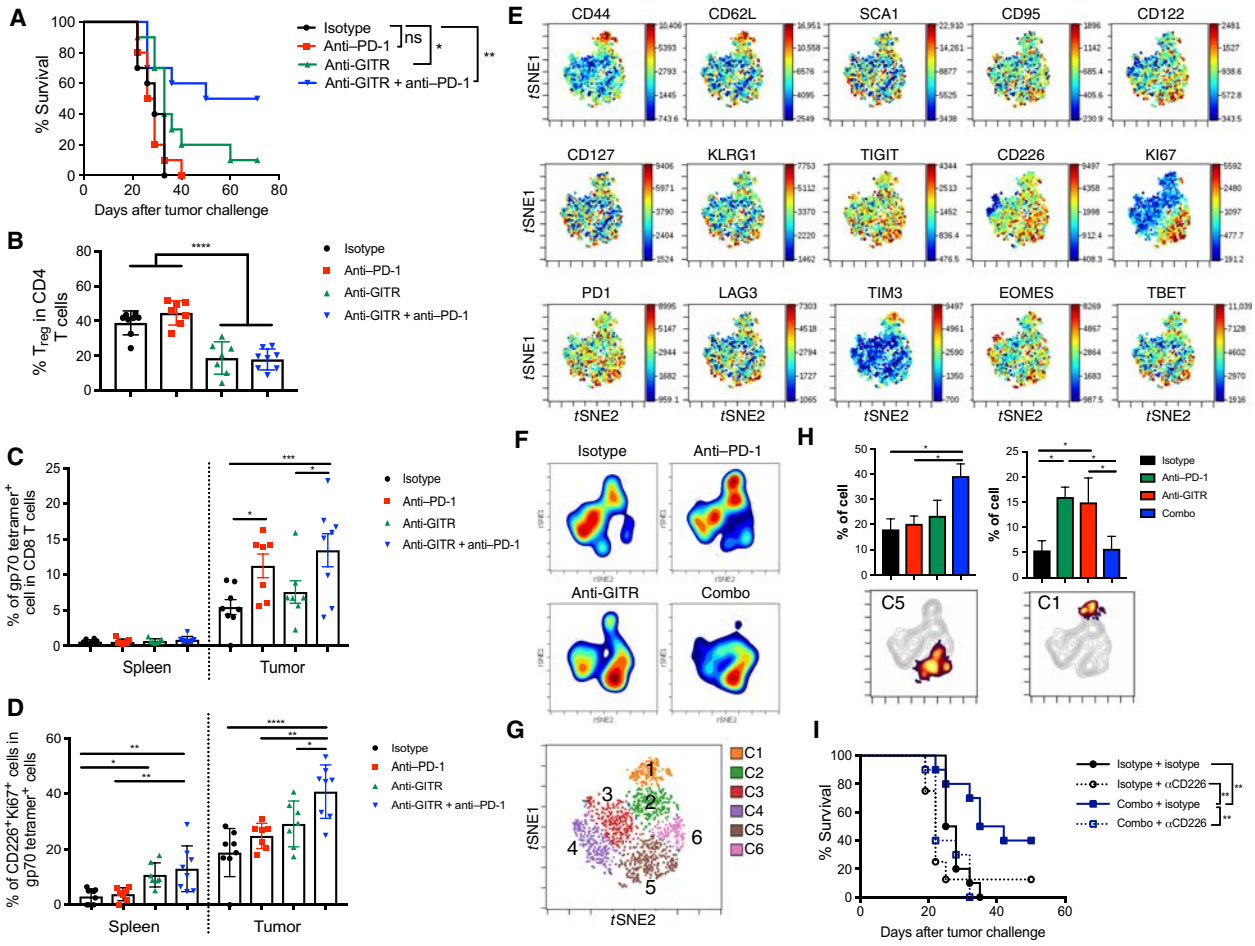

Fig. 6. CD226 signaling pathway is essential in mediating antitumor response induced by combination treatment in RENCA tumor model. (**A**) RENCA tumor–bearing mice were treated with either CD226-blocking Ab or isotype IgG before immunotherapy with anti-GITR and anti–PD-1 or isotype IgGs. The percentages of survival are shown here ($n = 8$ mice per group). ns, not significant. (**B**) Effect of Ab treatment on intratumoral T_{reg} frequency ($n = 7$ to 8 mice per group). (**C**) Frequency of tumor and spleen gp70-specific $CD8^+$ T cells from tumor-bearing mice treated with anti-GITR and/or anti–PD-1 Ab ($n = 8$ mice per group). (**D**) Frequency of $CD226^+Ki67^+$ cell in gp70-specific $CD8^+$ T cell population ($n = 7$ to 8 mice per group). (**E**) viSNE plot of tumor-infiltrating T cells overlaid with the expression of selected markers. (**F**) Density viSNE plot of gp70-specific tumor-infiltrating $CD8^+$ T cells from each treatment group day 11 after tumor challenge. (**G**) viSNE plot of RENCA infiltrating gp70-specific $CD8^+$ T cells overlaid with color-coded T cell clusters identified by SPADE. (**H**) Frequency of selected T cell clusters (means ± SEM). Indicated cluster was highlighted on viSNE plot below the bar graph. (**I**) RENCA tumor–bearing mice were treated with CD226-blocking Ab or isotype IgG before immunotherapy with anti-GITR and anti–PD-1 or isotype IgGs. The percentages of survival are shown here ($n = 10$ mice per group). * $P < 0.05$, ** $P < 0.01$, *** $P < 0.001$, **** $P < 0.0001$, one-way ANOVA with Tukey's test.

T cell state (Fig. 2, B to D). Last, we confirmed *CD226* as the most up-regulated gene upon combination treatment.

We developed a new bioinformatic pipeline rpsTCR that allowed us to selectively profile clonally expanded intratumoral $CD8^+$ T cells, which displayed distinct gene signature upon treatment with anti–PD-1 and/or anti-GITR Ab. Expression analysis of different subsets of intratumoral $CD8^+$ T cells (total, clonally expanded, or nonexpanded) across treatment groups revealed that *CD226* mRNA level was significantly increased by combination treatment in clonally expanded T cells, although this difference was diluted and lost in bulk and nonexpanded $CD8^+$ T cells. This observation stresses the importance of performing genome profiling on putative tumor-reactive clones (high-frequency T cell clones) to unmask critical gene changes. These genetic findings were validated at the protein level by comparing cell surface CD226 expression on tetramer-positive, antigen-specific intratumoral $CD8^+$ T cells after different Ab treatments. One potential limitation of the MC38 tumor model is that we tracked the clonally expanded $CD8^+$ T cells using a surrogate OVA antigen due to lack of reagents to track endogenous tumor antigen–specific $CD8^+$ T cells. However, we were able to validate the findings using the RENCA tumor model and endogenous tumor antigen–specific T cells.

Recently, both cis- and trans-inhibitory mechanisms have been proposed for the TIGIT/CD226 signaling pathway (*31*). Therefore, the net output of this pathway may result from the balance between the expression level of CD226 on $CD8^+$ T cells and TIGIT on both $CD8^+$ T cells and bystander lymphocytes. We found CD226 as a previously unidentified target for PD-1–initiated SHP2 dephosphorylation (Fig. 7) in addition to CD28 (*32*), thus revealing additional complexity of the PD-1 pathway. In addition, we showed that PD-1 blockade rescued CD226 dephosphorylation by PD-1–SHP2, whereas GITR agonism reduced TIGIT expression, which competes for CD155/PRV binding with CD226 (*42*). Therefore, only the combination treatment restored T cell effector function by favorably tipping the balance between CD226 and TIGIT leading to durable antitumor responses (model shown in Fig. 7).

In summary, the systematic approaches used in this study can shed light on important functional T cell regulatory pathways implicated in the synergy between two immunotherapeutic Abs, representing distinct immunotherapeutic modalities (costimulatory agonism and

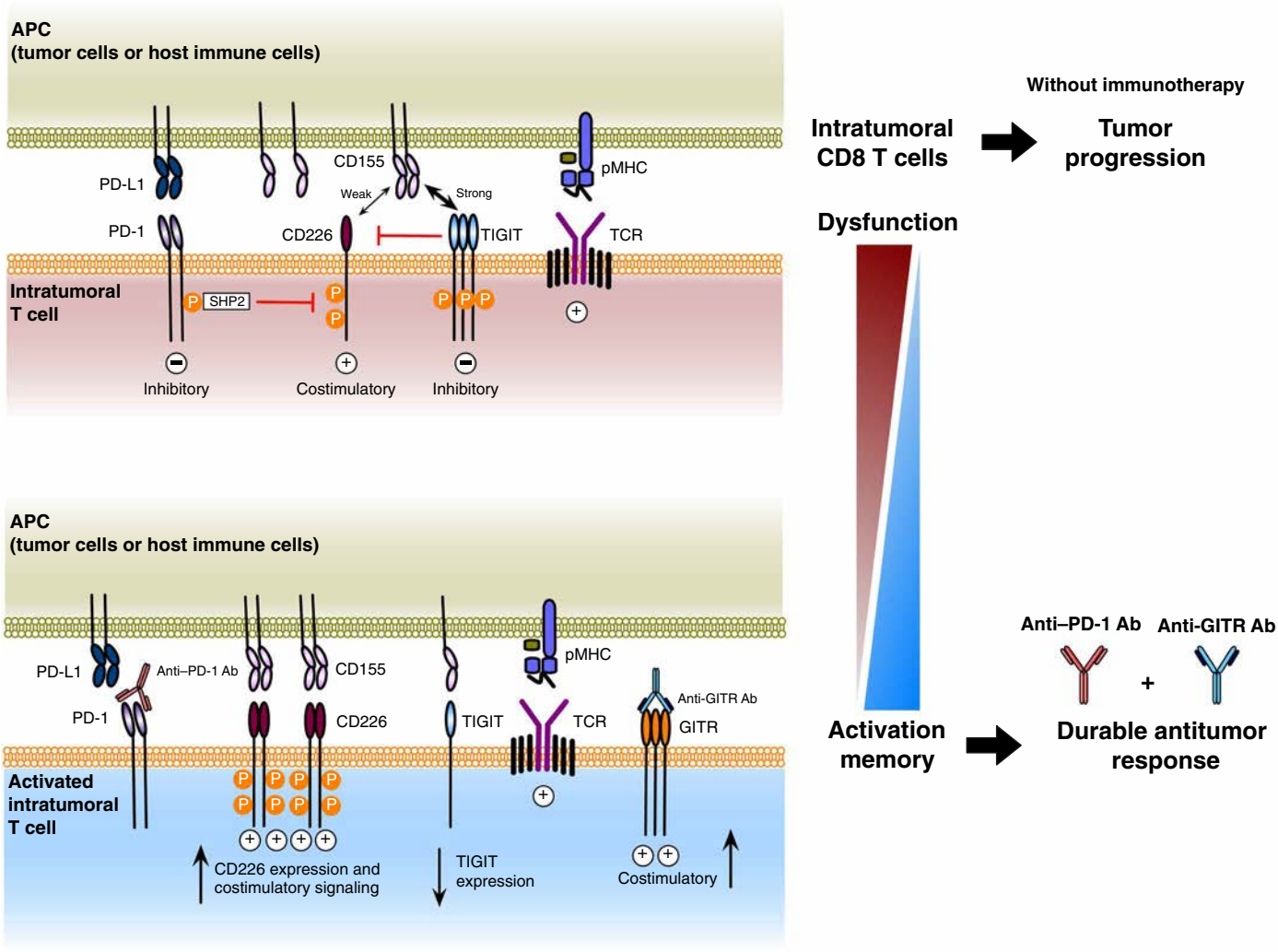

Fig. 7. Proposed model for anti–PD-1 and anti-GITR Ab combination therapy. pMHC, peptide–major histocompatibility complex; APC, antigen-presenting cells.

checkpoint inhibition). Similar methodology may be useful in future clinical trials of cancer immunotherapy to help unmask the molecular pathways driving durable antitumor responses.

MATERIALS AND METHODS

Study design

The aim of this study was to dissect the molecular and cellular mechanisms mediated by combination immunotherapy. Single-cell RNA-seq analysis study of tumor-infiltrating $CD8^+$ T cells was designed to identify the specific gene signature induced upon treatment. Single-cell suspensions were profiled by high-dimensional computational flow cytometry to identify phenotypic changes in cell populations. To validate our findings, we designed in vitro biochemistry experiments and additional in vivo studies using either genetically engineered mice or blocking Abs. Control and experimental treatments were administrated to age- and sex-matched mice. Investigators were blinded for tumor measurements. The number of experimental replicates is indicated in the figure legends.

Mice and treatments

Six- to eight-week-old female C57BL/6 and Balb/c mice were obtained from the Jackson laboratory. $CD226^{-/-}$ mice on a C57BL/6 background were generated at Regeneron Pharmaceuticals Inc. using the VelociGene method (*43*, *44*). Briefly, enhanced green fluorescent protein complementary DNA (cDNA) was inserted in-frame to the start codon, followed by a selection cassette that disrupts transcription of the gene body and results in a CD226 null allele. Heterozygous targeted mice were interbred to produce homozygous KO mice for study. All animals were maintained under pathogen-free conditions, and experiments were performed according to protocols approved by the Institute of Animal Care and Use Committee of Regeneron Pharmaceuticals Inc. For tumor studies, 3×10^5 MC38 or 1×10^6 RENCA cells were subcutaneously injected on the right flank of age-matched C57BL/6 or Balb/c, respectively. Six days after tumor implantation, mice (randomly distributed in different groups) were grouped on the basis of tumor size and treated by intraperitoneal injection with anti-GITR (5 mg/kg; DTA-1) and/or anti–PD-1 (RPM1-14) Ab or isotype control IgGs (rat IgG2b, LTF-2 and rat IgG2a, 2A3; Bio X Cell). Abs were administered again on day 13. Depletion/blocking Abs were given 1 to 2 days before immunotherapy. Perpendicular tumor diameters were measured blindly two to three times weekly using digital calipers (VWR, Radnor, PA). Volume was calculated using the formula $L \times W \times W \times 0.5$, where L is the longest dimension and W is the perpendicular dimension.

Flow cytometry

For flow cytometry analysis of in vivo experiments, blood, spleen, thymus, lymph node, and tumor were harvested on indicated days after treatment. Single-cell suspensions were prepared, and red blood cells were lysed using ACK lysis buffer (Thermo Fisher Scientific). Live/dead cell discrimination was performed using Live/Dead Fixable Blue Dead Cell Staining Kit (Thermo Fisher Scientific). Ag-specific $CD8^+$ T cells were detected with H-$2K^b$/OVA SIINFEKL-Pentamer (ProImmune) for MC38-OVA model and H-$2L^d$/MuLV gp70-SPSYVYHQF tetramer (MBL International) for RENCA model. For intracellular cytokine staining, cells were stimulated with or without SIINFEKL peptide for 36 hours and with a protein transport inhibitor (BD Biosciences) for the last 4 hours. After stimulation, cells were stained as described above for surface and intracellular proteins. To quantify cell numbers in tissue, a fixed number of CountBright absolute counting beads (Thermo Fisher Scientific) were added to each sample before acquiring. Samples were acquired on LSRFortessa X-20, LSR II, or Symphony (BD Biosciences) and analyzed using FlowJo (TreeStar) and Cytobank. Further details are in Supplementary Materials and Methods.

Single-cell sorting RNA-seq

FACS-sorted tumor and spleen $CD8^+$ T cells were mixed with C1 cell suspension reagent (Fluidigm) before loading onto a 5- to 10-μm C1 integrated fluidic circuit (Fluidigm). Cell lysing, reverse transcription, and cDNA amplification were performed on the C1 Single-Cell Auto Prep Integrated Fluidic Circuit, as specified by the manufacturer (protocol 100-7168 E1). The SMARTer Ultra Low RNA Kit (Clontech) was used for cDNA synthesis from the single cells. Illumina next-generation sequencing libraries were constructed using the Nextera XT DNA Sample Prep Kit (Illumina). Cells were sequenced on Illumina NextSeq (Illumina) by multiplexed single-read run with 75 cycles. Raw sequence data (BCL files) were converted to FASTQ format via Illumina Casava 1.8.2. Reads were decoded on the basis of their barcodes. Read quality was evaluated using FastQC (www.bioinformatics.babraham.ac.uk/projects/fastqc/). Further details are in Supplementary Materials and Methods.

LUV reconstitution and phosphotyrosine Western blot

LUVs reconstituted different components (ICOS, CD28, and CD226) involved in T cell signaling on the liposomes, together with LCK, ZAP70, SLP76, and PI3K as previously described (*45*–*47*). Proteins of interest were premixed at desired ratios in 1× reaction buffer containing bovine serum albumin (0.5 mg/ml) and then mixed with LUVs (1 mM total lipids) as described previously (*32*). Fifty micrograms of protein for each sample was used for the Western blot. Further details are in Supplementary Materials and Methods.

Statistical analysis

Sample sizes were chosen empirically to ensure adequate statistical power and were in the line with field standards for the techniques used in the study. Statistical significance was determined with analysis of variance (ANOVA) or unpaired two-tailed Student's t test, assuming unequal variance at $P < 0.05$ level of significance (or indicated in figure legends).

SUPPLEMENTARY MATERIALS

immunology.sciencemag.org/cgi/content/full/3/29/eaat7061/DC1

Fig. S1. T cell depletion with Abs.

Fig. S2. Bioinformatic pipeline rpsTCR.

Fig. S3. Combination therapy expands intratumoral high-frequency tumor-reactive $CD8^+$ T cell clones.

Fig. S4. Combination treatment expands tumor antigen–specific $CD8^+$ T cells with effector function.

Fig. S5. Mean fluorescence intensity of markers for dysfunctional cell clusters identified in Fig. 2.

Fig. S6. Mean fluorescence intensity of markers for effector/memory cell clusters identified in Fig. 3.

Fig. S7. TIGIT expression at single-cell RNA level and FACS analysis of TIGIT/CD226 expression level on different T cell subsets.

Fig. S8. GITR and PD-1 combination treatment significantly reduced highly activated T_{reg} subsets.

Fig. S9. GITR and PD-1 combination treatment induced intratumoral $CD8^+$ T cell subsets distinct from CD25 and PD-1 combination therapy.

Fig. S10. $CD226^{-/-}$ mice show normal T cell development and homeostatic function.

Fig. S11. Effectiveness of combination treatment does not rely on CD28, OX40, and 4-1BB pathway.
Fig. S12. Expression level of CD155.
Table S1. Negative controls for rpsTCR.
Table S2. Comparison of TCR detection rate.
Table S3. Selected genes differentially regulated by each treatment.
Table S4. Abs for flow cytometry.
Table S5. Primers for TCRα/β repertoire sequencing.
Table S6. Raw data.
References (*48*–*52*)

REFERENCES AND NOTES

1. S. C. Wei, C. R. Duffy, J. P. Allison, Fundamental mechanisms of immune checkpoint blockade therapy. *Cancer Discov.* **8**, 1069–1086 (2018).
2. Y. Iwai, J. Hamanishi, K. Chamoto, T. Honjo, Cancer immunotherapies targeting the PD-1 signaling pathway. *J. Biomed. Sci.* **24**, 26 (2017).
3. K. E. Pauken, M. A. Sammons, P. M. Odorizzi, S. Manne, J. Godec, O. Khan, A. M. Drake, Z. Chen, D. R. Sen, M. Kurachi, R. A. Barnitz, C. Bartman, B. Bengsch, A. C. Huang, J. M. Schenkel, G. Vahedi, W. N. Haining, S. L. Berger, E. J. Wherry, Epigenetic stability of exhausted T cells limits durability of reinvigoration by PD-1 blockade. *Science* **354**, 1160–1165 (2016).
4. D. R. Sen, J. Kaminski, R. A. Barnitz, M. Kurachi, U. Gerdemann, K. B. Yates, H.-W. Tsao, J. Godec, M. W. LaFleur, F. D. Brown, P. Tonnerre, R. T. Chung, D. C. Tully, T. M. Allen, N. Frahm, G. M. Lauer, E. J. Wherry, N. Yosef, W. N. Haining, The epigenetic landscape of T cell exhaustion. *Science* **354**, 1165–1169 (2016).
5. S. Yao, Y. Zhu, L. Chen, Advances in targeting cell surface signalling molecules for immune modulation. *Nat. Rev. Drug Discov.* **12**, 130–146 (2013).
6. D. A. Knee, B. Hewes, J. L. Brogdon, Rationale for anti-GITR cancer immunotherapy. *Eur. J. Cancer* **67**, 1–10 (2016).
7. L. L. Siu, N. Steeghs, T. Meniawy, M. Joerger, J. L. Spratlin, S. Rottey, A. Nagrial, A. Cooper, R. Meier, X. Guan, P. Phillips, G. Bajaj, J. Gokemeijer, A. J. Korman, K. L. Aung, M. S. Carlino, Preliminary results of a phase I/IIa study of BMS-986156 (glucocorticoid-induced tumor necrosis factor receptor–related gene [GITR] agonist), alone and in combination with nivolumab in pts with advanced solid tumors. *J. Clin. Oncol.* **35**, 104 (2017).
8. C. T.-S. Victor, A. J. Rech, A. Maity, R. Rengan, K. E. Pauken, E. Stelekati, J. L. Benci, B. Xu, H. Dada, P. M. Odorizzi, R. S. Herati, K. D. Mansfield, D. Patsch, R. K. Amaravadi, L. M. Schuchter, H. Ishwaran, R. Mick, D. A. Pryma, X. Xu, M. D. Feldman, T. C. Gangadhar, S. M. Hahn, E. J. Wherry, R. H. Vonderheide, A. J. Minn, Radiation and dual checkpoint blockade activate non-redundant immune mechanisms in cancer. *Nature*, 1–18 (2015).
9. L. Lu, X. Xu, B. Zhang, R. Zhang, H. Ji, X. Wang, Combined PD-1 blockade and GITR triggering induce a potent antitumor immunity in murine cancer models and synergizes with chemotherapeutic drugs. *J. Transl. Med.* **12**, 36 (2014).
10. S. I. S. Mosely, J. E. Prime, R. C. A. Sainson, J.-O. Koopmann, D. Y. Q. Wang, D. M. Greenawalt, M. J. Ahdesmaki, R. Leyland, S. Mullins, L. Pacelli, D. Marcus, J. Anderton, A. Watkins, J. Coates Ulrichsen, P. Brohawn, B. W. Higgs, M. McCourt, H. Jones, J. A. Harper, M. Morrow, V. Valge-Archer, R. Stewart, S. J. Dovedi, R. W. Wilkinson, Rational selection of syngeneic preclinical tumor models for immunotherapeutic drug discovery. *Cancer Immunol. Res.* **5**, 29–41 (2017).
11. S. Chen, L.-F. Lee, T. S. Fisher, B. Jessen, M. Elliott, W. Evering, K. Logronio, G. H. Tu, K. Tsaparikos, X. Li, H. Wang, C. Ying, M. Xiong, T. VanArsdale, J. C. Lin, Combination of 4-1BB agonist and PD-1 antagonist promotes antitumor effector/memory CD8 T cells in a poorly immunogenic tumor model. *Cancer Immunol. Res.* **3**, 149–160 (2015).
12. A. E. Mahne, S. Mauze, B. Joyce-Shaikh, J. Xia, E. P. Bowman, A. M. Beebe, D. J. Cua, R. Jain, Dual roles for regulatory T-cell depletion and costimulatory signaling in agonistic GITR targeting for tumor immunotherapy. *Cancer Res.* **77**, 1108–1118 (2017).
13. Y. Bulliard, R. Jolicoeur, M. Windman, S. M. Rue, S. Ettenberg, D. A. Knee, N. S. Wilson, G. Dranoff, J. L. Brogdon, Activating Fc γ receptors contribute to the antitumor activities of immunoregulatory receptor-targeting antibodies. *J. Exp. Med.* **210**, 1685–1693 (2013).
14. E. Cha, M. Klinger, Y. Hou, C. Cummings, A. Ribas, M. Faham, L. Fong, Improved survival with T cell clonotype stability after anti-CTLA-4 treatment in cancer patients. *Sci. Transl. Med.* **6**, 238ra70 (2014).
15. A. Han, J. Glanville, L. Hansmann, M. M. Davis, Linking T-cell receptor sequence to functional phenotype at the single-cell level. *Nat. Biotechnol.* **32**, 684–692 (2014).
16. L. Robert, C. Harview, R. Emerson, X. Wang, S. Mok, B. Homet, B. Comin-Anduix, R. C. Koya, H. Robins, P. C. Tumeh, A. Ribas, Distinct immunological mechanisms of CTLA-4 and PD-1 blockade revealed by analyzing TCR usage in blood lymphocytes. *Oncoimmunology* **3**, e29244 (2014).
17. M. Singer, C. Wang, L. Cong, N. D. Marjanovic, M. S. Kowalczyk, H. Zhang, J. Nyman, K. Sakuishi, S. Kurtulus, D. Gennert, J. Xia, J. Y. H. Kwon, J. Nevin, R. H. Herbst, I. Yanai, O. Rozenblatt-Rosen, V. K. Kuchroo, A. Regev, A. C. Anderson, A distinct gene module for dysfunction uncoupled from activation in tumor-infiltrating T cells. *Cell* **166**, 1500–1511.e9 (2016).
18. C. C. Ku, M. Murakami, A. Sakamoto, J. Kappler, P. Marrack, Control of homeostasis of $CD8^+$ memory T cells by opposing cytokines. *Science* **288**, 675–678 (2000).
19. S. Choi, C. Warzecha, E. Zvezdova, J. Lee, J. Argenty, R. Lesourne, L. Aravind, P. E. Love, THEMIS enhances TCR signaling and enables positive selection by selective inhibition of the phosphatase SHP-1. *Nat. Immunol.* **18**, 433–441 (2017).
20. S. Gilfillan, C. J. Chan, M. Cella, N. M. Haynes, A. S. Rapaport, K. S. Boles, D. M. Andrews, M. J. Smyth, M. Colonna, DNAM-1 promotes activation of cytotoxic lymphocytes by nonprofessional antigen-presenting cells and tumors. *J. Exp. Med.* **205**, 2965–2973 (2008).
21. D. Peter, S. L. C. Jin, M. Conti, A. Hatzelmann, C. Zitt, Differential expression and function of phosphodiesterase 4 (PDE4) subtypes in human primary $CD4^+$ T cells: Predominant role of PDE4D. *J. Immunol.* **178**, 4820–4831 (2007).
22. M. Villalba, K. Bi, F. Rodriguez, Y. Tanaka, S. Schoenberger, A. Altman, Vav1/Rac-dependent actin cytoskeleton reorganization is required for lipid raft clustering in T cells. *J. Cell Biol.* **155**, 331–338 (2001).
23. C. Y. Yang, J. A. Best, J. Knell, E. Yang, A. D. Sheridan, A. K. Jesionek, H. S. Li, R. R. Rivera, K. C. Lind, L. M. D'Cruz, S. S. Watowich, C. Murre, A. W. Goldrath, The transcriptional regulators Id2 and Id3 control the formation of distinct memory $CD8^+$ T cell subsets. *Nat. Immunol.* **12**, 1221–1229 (2011).
24. A. Schietinger, M. Philip, V. E. Krisnawan, E. Y. Chiu, J. J. Delrow, R. S. Basom, P. Lauer, D. G. Brockstedt, S. E. Knoblaugh, G. J. Hämmerling, T. D. Schell, N. Garbi, P. D. Greenberg, Tumor-specific T cell dysfunction is a dynamic antigen-driven differentiation program initiated early during tumorigenesis. *Immunity* **45**, 389–401 (2016).
25. E.-A. D. Amir, K. L. Davis, M. D. Tadmor, E. F. Simonds, J. H. Levine, S. C. Bendall, D. K. Shenfeld, S. Krishnaswamy, G. P. Nolan, D. Pe'er, viSNE enables visualization of high dimensional single-cell data and reveals phenotypic heterogeneity of leukemia. *Nat. Biotechnol.* **31**, 545–552 (2013).
26. P. Qiu, E. F. Simonds, S. C. Bendall, K. D. Gibbs Jr., R. V. Bruggner, M. D. Linderman, K. Sachs, G. P. Nolan, S. K. Plevritis, Extracting a cellular hierarchy from high-dimensional cytometry data with SPADE. *Nat. Biotechnol.* **29**, 886–891 (2011).
27. M. Yadav, S. Jhunjhunwala, Q. T. Phung, P. Lupardus, J. Tanguay, S. Bumbaca, C. Franci, T. K. Cheung, J. Fritsche, T. Weinschenk, Z. Modrusan, I. Mellman, J. R. Lill, L. Delamarre, Predicting immunogenic tumour mutations by combining mass spectrometry and exome sequencing. *Nature* **515**, 572–576 (2014).
28. B. Homet Moreno, J. M. Zaretsky, A. Garcia-Diaz, J. Tsoi, G. Parisi, L. Robert, K. Meeth, A. Ndoye, M. W. Bosenberg, A. T. Weeraratna, T. G. Graeber, B. Comin-Anduix, S. Hu-Lieskovan, A. Ribas, Response to programmed cell death-1 blockade in a murine melanoma syngeneic model requires costimulation, CD4, and CD8 T cells. *Cancer Immunol. Res.* **4**, 845–857 (2016).
29. V. R. Buchholz, T. N. M. Schumacher, D. H. Busch, T cell fate at the single-cell level. *Annu. Rev. Immunol.* **34**, 65–92 (2016).
30. R. J. Johnston, L. Comps-Agrar, J. Hackney, X. Yu, M. Huseni, Y. Yang, S. Park, V. Javinal, H. Chiu, B. Irving, D. L. Eaton, J. L. Grogan, The immunoreceptor TIGIT regulates antitumor and antiviral $CD8^+$ T cell effector function. *Cancer Cell* **26**, 923–937 (2014).
31. K. E. Pauken, E. J. Wherry, TIGIT and CD226: Tipping the balance between costimulatory and coinhibitory molecules to augment the cancer immunotherapy toolkit. *Cancer Cell* **26**, 785–787 (2014).
32. E. Hui, J. Cheung, J. Zhu, X. Su, M. J. Taylor, H. A. Wallweber, D. K. Sasmal, J. Huang, J. M. Kim, I. Mellman, R. D. Vale, T cell costimulatory receptor CD28 is a primary target for PD-1-mediated inhibition. *Science* **355**, 1428–1433 (2017).
33. M. F. Bachmann, K. McKall-Faienza, R. Schmits, D. Bouchard, J. Beach, D. E. Speiser, T. W. Mak, P. S. Ohashi, Distinct roles for LFA-1 and CD28 during activation of naive T cells: Adhesion versus costimulation. *Immunity* **7**, 549–557 (1997).
34. K. Shibuya, J. Shirakawa, T. Kameyama, S.-I. Honda, S. Tahara-Hanaoka, A. Miyamoto, M. Onodera, T. Sumida, H. Nakauchi, H. Miyoshi, A. Shibuya, CD226 (DNAM-1) is involved in lymphocyte function-associated antigen 1 costimulatory signal for naive T cell differentiation and proliferation. *J. Exp. Med.* **198**, 1829–1839 (2003).
35. N. Joller, J. P. Hafler, B. Brynedal, N. Kassam, S. Spoerl, S. D. Levin, A. H. Sharpe, V. K. Kuchroo, Cutting edge: TIGIT has T cell-intrinsic inhibitory functions. *J. Immunol.* **186**, 1338–1342 (2011).
36. N. Joller, E. Lozano, P. R. Burkett, B. Patel, S. Xiao, C. Zhu, J. Xia, T. G. Tan, E. Sefik, V. Yajnik, A. H. Sharpe, F. J. Quintana, D. Mathis, C. Benoist, D. A. Hafler, V. K. Kuchroo, Treg cells expressing the coinhibitory molecule TIGIT selectively inhibit proinflammatory Th1 and Th17 cell responses. *Immunity* **40**, 569–581 (2014).
37. A. C. Anderson, N. Joller, V. K. Kuchroo, Lag-3, Tim-3, and TIGIT: Co-inhibitory receptors with specialized functions in immune regulation. *Immunity* **44**, 989–1004 (2016).
38. M. M. Gubin, X. Zhang, H. Schuster, E. Caron, J. P. Ward, T. Noguchi, Y. Ivanova, J. Hundal, C. D. Arthur, W.-J. Krebber, G. E. Mulder, M. Toebes, M. D. Vesely, S. S. K. Lam, A. J. Korman, J. P. Allison, G. J. Freeman, A. H. Sharpe, E. L. Pearce, T. N. Schumacher, R. Aebersold,

H.-G. Rammensee, C. J. M. Melief, E. R. Mardis, W. E. Gillanders, M. N. Artyomov, R. D. Schreiber, Checkpoint blockade cancer immunotherapy targets tumour-specific mutant antigens. *Nature* **515**, 577–581 (2014).
39. B. Bengsch, A. L. Johnson, M. Kurachi, P. M. Odorizzi, K. E. Pauken, J. Attanasio, E. Stelekati, L. M. McLane, M. A. Paley, G. M. Delgoffe, E. J. Wherry, Bioenergetic insufficiencies due to metabolic alterations regulated by the inhibitory receptor PD-1 are an early driver of $CD8^+$ T cell exhaustion. *Immunity* **45**, 358–373 (2016).
40. R. J. Johnston, X. Yu, J. L. Grogan, The checkpoint inhibitor TIGIT limits antitumor and antiviral $CD8^+$ T cell responses. *Oncoimmunology* **4**, e1036214 (2015).
41. A. O. Kamphorst, A. Wieland, T. Nasti, S. Yang, R. Zhang, D. L. Barber, B. T. Konieczny, C. Z. Daugherty, L. Koenig, K. Yu, G. L. Sica, A. H. Sharpe, G. J. Freeman, B. R. Blazar, L. A. Turka, T. K. Owonikoko, R. Pillai, S. S. Ramalingam, K. Araki, R. Ahmed, Rescue of exhausted CD8 T cells by PD-1–targeted therapies is CD28-dependent. *Science*, eaaf0683 (2017).
42. E. Lozano, M. Dominguez-Villar, V. Kuchroo, D. A. Hafler, The TIGIT/CD226 axis regulates human T cell function. *J. Immunol.* **188**, 3869–3875 (2012).
43. D. M. Valenzuela, A. J. Murphy, D. Frendewey, N. W. Gale, A. N. Economides, W. Auerbach, W. T. Poueymirou, N. C. Adams, J. Rojas, J. Yasenchak, R. Chernomorsky, M. Boucher, A. L. Elsasser, L. Esau, J. Zheng, J. A. Griffiths, X. Wang, H. Su, Y. Xue, M. G. Dominguez, I. Noguera, R. Torres, L. E. Macdonald, A. F. Stewart, T. M. DeChiara, G. D. Yancopoulos, High-throughput engineering of the mouse genome coupled with high-resolution expression analysis. *Nat. Biotechnol.* **21**, 652–659 (2003).
44. W. T. Poueymirou, W. Auerbach, D. Frendewey, J. F. Hickey, J. M. Escaravage, L. Esau, A. T. Doré, S. Stevens, N. C. Adams, M. G. Dominguez, N. W. Gale, G. D. Yancopoulos, T. M. DeChiara, D. M. Valenzuela, F0 generation mice fully derived from gene-targeted embryonic stem cells allowing immediate phenotypic analyses. *Nat. Biotechnol.* **25**, 91–99 (2007).
45. F. Pagès, M. Ragueneau, R. Rottapel, A. Truneh, J. Nunes, J. Imbert, D. Olive, Binding of phosphatidyl-inositol-3-OH kinase to CD28 is required for T-cell signalling. *Nature* **369**, 327–329 (1994).
46. H. Wang, T. A. Kadlecek, B. B. Au-Yeung, H. E. S. Goodfellow, L.-Y. Hsu, T. S. Freedman, A. Weiss, ZAP-70: An essential kinase in T-cell signaling. *Cold Spring Harb. Perspect. Biol.* **2**, a002279 (2010).
47. W. Zhang, J. Sloan-Lancaster, J. Kitchen, R. P. Trible, L. E. Samelson, LAT: The ZAP-70 tyrosine kinase substrate that links T cell receptor to cellular activation. *Cell* **92**, 83–92 (1998).
48. R. V. Bruggner, B. Bodenmiller, D. L. Dill, R. J. Tibshirani, G. P. Nolan, Automated identification of stratifying signatures in cellular subpopulations. *Proc. Natl. Acad. Sci. U. S. A.* **111**, E2770–E2777 (2014).
49. C. Trapnell, L. Pachter, S. L. Salzberg, TopHat: Discovering splice junctions with RNA-Seq. *Bioinformatics* **25**, 1105–1111 (2009).
50. X. Yang, D. Liu, F. Liu, J. Wu, J. Zou, X. Xiao, F. Zhao, B. Zhu, HTQC: A fast quality control toolkit for Illumina sequencing data. *BMC Bioinform.* **14**, 33 (2013).
51. X. Yang, D. Liu, N. Lv, F. Zhao, F. Liu, J. Zou, Y. Chen, X. Xiao, J. Wu, P. Liu, J. Gao, Y. Hu, Y. Shi, J. Liu, R. Zhang, C. Chen, J. Ma, G. F. Gao, B. Zhu, TCRklass: A new K-string-based algorithm for human and mouse TCR repertoire characterization. *J. Immunol.* **194**, 446–454 (2014).
52. A. Han, J. Glanville, L. Hansmann, M. M. Davis, Linking T-cell receptor sequence to functional phenotype at the single-cell level. *Nat. Biotechnol.* **32**, 684–692 (2014).

Acknowledgments: We acknowledge J. Napetschnig for project management and K. Daniels, S. Nandor, and P. Burfeind for FACS. **Funding:** This research was funded by Regeneron Pharmaceuticals Inc. Some components of this project were funded in part by Sanofi. **Author contributions:** B.W. and D.S. designed the study. B.W., J.G., P.P., E.M.O., I.R., Q.W., J. Wei, J. Waite, M.N., C.A., and Y.W. performed experiments. B.W., W.Z., and D.S. analyzed data. W.Z. performed the bioinformatics analysis and provided the statistical consultation. S.B., J.S., and W.P. generated and provided genetically modified mice for experiments. B.W., W.Z., M.A.S., and D.S. wrote the manuscript. V.J., D.M., L.M., T.R., C.G., G.D.Y., A.J.M., and D.S. gave technical support and conceptual advice. **Competing interests:** All authors are employees of Regeneron Pharmaceuticals Inc. D.S. and B.W. are inventors on a pending U.S. patent application (20170355774; "Anti-GITR Antibodies and Uses Thereof"). B.W. and W.Z. are inventors on a pending U.S. patent application (20180201991; "Systems and Methods for Sequencing T Cell Receptors and Uses Thereof"). **Data and materials availability:** RNA-seq data are available from the Gene Expression Omnibus under accession number GSE120909.

Submitted 26 March 2018
Accepted 11 October 2018
Published 2 November 2018
10.1126/sciimmunol.aat7061

Citation: B. Wang, W. Zhang, V. Jankovic, J. Golubov, P. Poon, E. M. Oswald, C. Gurer, J. Wei, I. Ramos, Q. Wu, J. Waite, M. Ni, C. Adler, Y. Wei, L. Macdonald, T. Rowlands, S. Brydges, J. Siao, W. Poueymirou, D. MacDonald, G. D. Yancopoulos, M. A. Sleeman, A. J. Murphy, D. Skokos, Combination cancer immunotherapy targeting PD-1 and GITR can rescue $CD8^+$ T cell dysfunction and maintain memory phenotype. *Sci. Immunol.* **3**, eaat7061 (2018).

Science Immunology

Combination cancer immunotherapy targeting PD-1 and GITR can rescue CD8$^+$ T cell dysfunction and maintain memory phenotype

Bei Wang, Wen Zhang, Vladimir Jankovic, Jacquelynn Golubov, Patrick Poon, Erin M. Oswald, Cagan Gurer, Joyce Wei, Ilyssa Ramos, Qi Wu, Janelle Waite, Min Ni, Christina Adler, Yi Wei, Lynn Macdonald, Tracey Rowlands, Susannah Brydges, Jean Siao, William Poueymirou, Douglas MacDonald, George D. Yancopoulos, Matthew A. Sleeman, Andrew J. Murphy and Dimitris Skokos

Sci. Immunol. **3**, eaat7061.
DOI: 10.1126/sciimmunol.aat7061

Tandem immunotherapy achieves synergy

Immune checkpoint inhibitor therapies bolster the antitumor activity of CD8$^+$ T lymphocytes. Wang *et al*. used single-cell analysis of tumor-infiltrating lymphocytes to probe the mechanisms responsible for their observation that a combination of blocking anti–PD-1 and agonist anti-GITR antibodies enhanced tumor control in mouse cancer models. This combination immunotherapy led to a synergistic increase in tumor antigen–specific memory precursor effector T cells dependent on availability of the CD226 costimulatory pathway. Biochemical studies in liposomes identified CD226 as an additional target of dephosphorylation mediated by the PD-1–SHP2 complex. These results provide a mechanistic rationale for conducting further clinical trials of combined anti-GITR and anti–PD-1 immunotherapy in human cancer.

Science Immunology (ISSN 2470-9468) is published by the American Association for the Advancement of Science, 1200 New York Avenue NW, Washington, DC 20005.